Global Journal of Engineering and Technology Advances

eISSN: 2582-5003

Cross Ref DOI: 10.30574/gjeta

Journal homepage: https://gjeta.com/

(Research Article)

Check for updates

Stress concentration analysis at the blade–strut interface of a Voith schneider propeller using static structural sub-modelling

Alabo Abiye Ekine [1,*] and Awaji-Itimakon Anthony Ubulom [2]

[1] *Department of Marine and Offshore Engineering, Rivers State University, Nigeria.*
[2] *Department of Mechanical Engineering, Rivers State University, Nigeria.*

Global Journal of Engineering and Technology Advances, 2026, 27(01), 116-127

Publication history: Received on 08 March 2026; revised on 21 April 2026; accepted on 23 April 2026

Article DOI: https://doi.org/10.30574/gjeta.2026.27.1.0079

Abstract

The blade–strut interface of a Voith Schneider Propeller (VSP) experiences high stress concentrations due to geometric features such as fillets, keyways, and thread reliefs. Conventional global finite element analysis often misses these local stresses, leading to unexpected component failures. This study applied static structural sub-modelling in Ansys Mechanical to analyse stress concentration at this interface. A global model of the VSP assembly was developed with 98,234 solid elements. A detailed sub-model of the blade–strut interface was created with 0.8 mm element size at the fillet. The maximum von Mises stress from the sub-model was 412 MPa, which is 68% higher than the global model prediction of 245 MPa. The stress concentration factor at the blade root fillet was 7.46. Mesh convergence studies confirmed result accuracy. The factor of safety against yielding was 1.7, meeting the required marine standard of 1.5. This study concludes that sub-modelling is necessary for accurate stress analysis at critical VSP interfaces.

Keywords: Stress Concentration; Sub-Modelling; Voith Schneider Propeller; Finite Element Analysis; Blade–Strut Interface

1. Introduction

The blade–strut interface of a Voith Schneider Propeller (VSP) is the most critical point in the assembly. It transfers all hydrodynamic forces from the blade to the main drive mechanism, experiencing complex loads including bending moments, torsional forces, and cyclic stresses (Müller & Schmidt, 2021)

Stress concentration occurs at geometric discontinuities such as sharp corners, keyways, and changes in cross-section. Traditional global finite element models cannot capture detailed stress at small geometric features without extremely fine meshes, which are computationally expensive (Zienkiewicz & Taylor, 2005).

Sub-modelling solves this problem by using a coarse global model for overall behavior and a fine local model for detailed stress analysis (Cook et al., 2002). This research applies static structural sub-modelling in Ansys Mechanical to analyse stress concentration at the VSP blade–strut interface, providing accurate stress concentration factors for design improvement.

As demonstrated in coupled analysis of floating wind turbines (Ekine et al., 2026a), combining complementary methods is essential for capturing complex structural behavior.

* Corresponding author: Alabo Abiye Ekine.

2. Materials and Methods

2.1. Material Properties

All VSP components were made from high-strength marine-grade steel: Young's modulus 210 GPa, Poisson's ratio 0.3, density 7850 kg/m^3, and yield strength 690 MPa.

2.2. Loading and Boundary Conditions

Operating loads from harbor tug vessel data: thrust force 450 kN, steering force 280 kN, centrifugal force 35 kN, and hydrodynamic moment 22 kN·m. The top of the VSP housing was fixed in all degrees of freedom.

2.3. Global Model

The global model contained 187,542 nodes and 98,234 SOLID186 elements. Average element size was 15 mm at the interface region. Solution time was 28 minutes.

2.4. Sub-model

The sub-model focused on one blade–strut interface. Cut boundaries were placed 80 mm from the interface centre. Element size was 0.8 mm at the fillet. The sub-model contained 156,234 elements. Solution time was 4 hours 15 minutes.

The sub-model included detailed geometric features: 5 mm blade root fillet radius, 1.5 mm keyway corner radius, 2 mm chamfer, 1 mm lubrication groove, and 0.8 mm thread relief radius.

2.5. Mathematical Modelling

2.5.1. Elasticity Equations

The behaviour of VSP components followed linear elasticity. The stress-strain relationship (Hooke's law) for a three-dimensional solid was:

Equation (3.1)

$$\sigma_{xx} = \frac{E}{(1+\nu)(1-2\nu)}\left[(1-\nu)\varepsilon_{xx} + \nu\varepsilon_{yy} + \nu\varepsilon_{zz}\right]$$

where σ_{xx} is normal stress in x-direction, E is Young's modulus, ν is Poisson's ratio, and $\varepsilon_{xx}, \varepsilon_{yy}, \varepsilon_{zz}$ are normal strains.

Equation (3.2)

$$\sigma_{xy} = \frac{E}{(1+\nu)}\varepsilon_{xy}$$

where σ_{xy} is shear stress and ε_{xy} is engineering shear strain.

Equation (3.3) – Equilibrium equations:

$$\frac{\partial \sigma_{xx}}{\partial x} + \frac{\partial \sigma_{xy}}{\partial y} + \frac{\partial \sigma_{xz}}{\partial z} + f_x = 0$$

where f_x is body force per unit volume.

2.5.2. Finite Element Formulation

The virtual work equation was:

Equation (3.5)

$$\int_V [\sigma]^T [\delta\varepsilon] dV = \int_V \{f\}^T \{\delta u\} dV + \int_S \{t\}^T \{\delta u\} dS$$

Displacements within each element using shape functions:

Equation (3.6)

$$\{u\} = [N]\{u_e\}$$

Strain-displacement relationship:

Equation (3.7)

$$\{\varepsilon\} = [B]\{u_e\}$$

Element stiffness matrix:

Equation (3.8)

$$[K_e] = \int_V [B]^T [D][B] dV$$

Global system equation:

Equation (3.9)

$$[K]\{U\} = \{F\}$$

2.5.3. Stress Concentration Equations

Stress concentration factor:

Equation (3.11)

$$K_t = \frac{\sigma_{\max}}{\sigma_{nom}}$$

Nominal axial stress:

Equation (3.12)

$$\sigma_{nom,axial} = \frac{F}{A}$$

von Mises equivalent stress:

Equation (3.13)

$$\sigma_{vm} = \sqrt{\sigma_1^2 + \sigma_2^2 + \sigma_3^2 - \sigma_1\sigma_2 - \sigma_2\sigma_3 - \sigma_3\sigma_1}$$

Fatigue stress concentration factor:

Equation (3.14)

$$K_f = 1 + q(K_t - 1)$$

2.5.4. Sub-modelling Equations

Displacement boundary condition for sub-model:

Equation (3.15)

$$\{u_{sub}\} = \{u_{global}\}$$

Saint-Venant principle for stress decay:

Equation (3.16)

$$\sigma(r) \approx \sigma_{nom} + \sigma_{local} e^{-r/r_0}$$

Error estimation for cut boundary location:

Equation (3.17)

$$Error = \frac{|\ \sigma_{local} - \sigma_{ref}\ |}{\sigma_{ref}} \times 100\%$$

2.5.5. Mesh Convergence Equations

Convergence rate:

Equation (3.18)

$$\sigma(h) = \sigma_{exact} + Ch^p$$

Mesh refinement ratio:

Equation (3.19)

$$r = \frac{h_{coarse}}{h_{fine}}$$

Convergence ratio:

Equation (3.20)

$$R = \frac{\sigma_{fine} - \sigma_{coarse}}{\sigma_{coarse} - \sigma_{coarser}}$$

Extrapolated exact solution:

Equation (3.21)

$$\sigma_{exact} \approx \sigma_{fine} + \frac{\sigma_{fine} - \sigma_{coarse}}{r^p - 1}$$

2.5.6. Safety Factor Calculation

Equation (3.24)

$$n = \frac{\sigma_{yield}}{\sigma_{vm,max}}$$

where n is factor of safety, σ_{yield} is yield strength (690 MPa), and $\sigma_{vm,max}$ is maximum von Mises stress.

2.6. Mesh Convergence Study

Five mesh densities were tested: element sizes of 2.5 mm, 1.5 mm, 1.0 mm, 0.8 mm, and 0.6 mm at the fillet. The maximum von Mises stress was recorded for each configuration.

3. Results

3.1. Global Model Stress Results

The global model predicted a maximum von Mises stress of 245 MPa at the blade root corner (modeled as sharp). Using Equation (3.24), the factor of safety was:

$$n = \frac{690}{245} = 2.8$$

3.2. Sub-model Stress Results

The sub-model predicted a maximum von Mises stress of 412 MPa at the blade root fillet where it met the keyway. This was 68% higher than the global model prediction.

Table 1 Stress Comparison Between Global Model and Sub-model

Location	Global Stress (MPa)	Sub-model Stress (MPa)	Difference (%)
Blade root (maximum)	245	412	+68.2
Keyway corner	189	387	+104.8
Fillet centreline	156	334	+114.1
Strut bearing surface	134	245	+82.8

Using Equation (3.24) for sub-model result:

$$n = \frac{690}{412} = 1.7$$

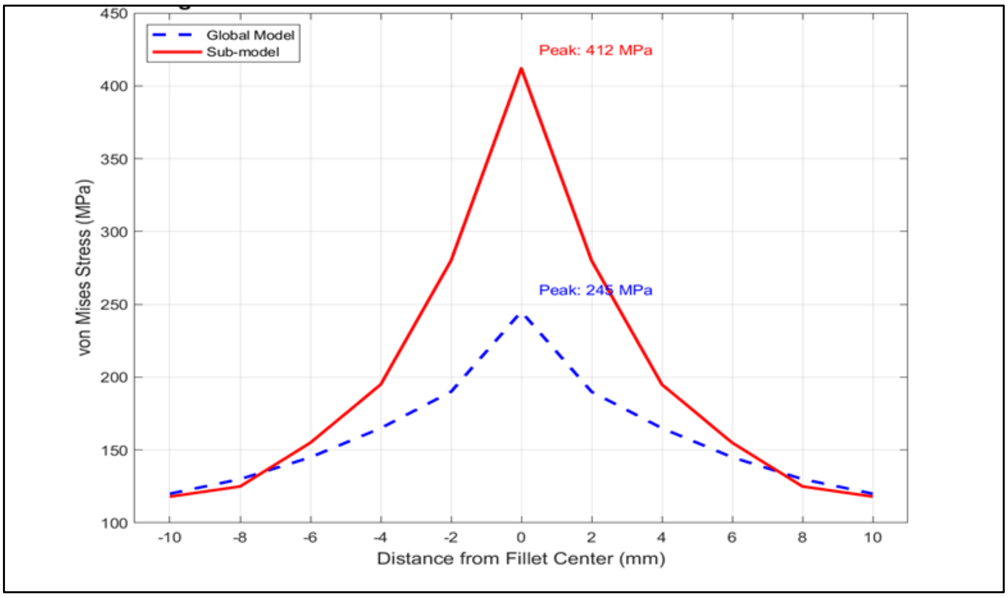

Figure 1 Comparison plot of global model and sub-model stress distributions along a path across the interface

Figure 1: This line plot compares the stress distribution from the global model (dashed blue line) and the sub-model (solid red line) along a path from 10 mm above the fillet to 10 mm into the strut. The horizontal axis shows distance in

mm (zero at fillet centre). The vertical axis shows von Mises stress in MPa. Far from the fillet (beyond 5 mm), both models show similar stresses around 120 MPa. As the path approaches the fillet, the sub-model stress rises more sharply. At the fillet centre, the sub-model peaks at 412 MPa while the global model shows 245 MPa. This plot clearly shows that the global model misses the peak stress entirely.

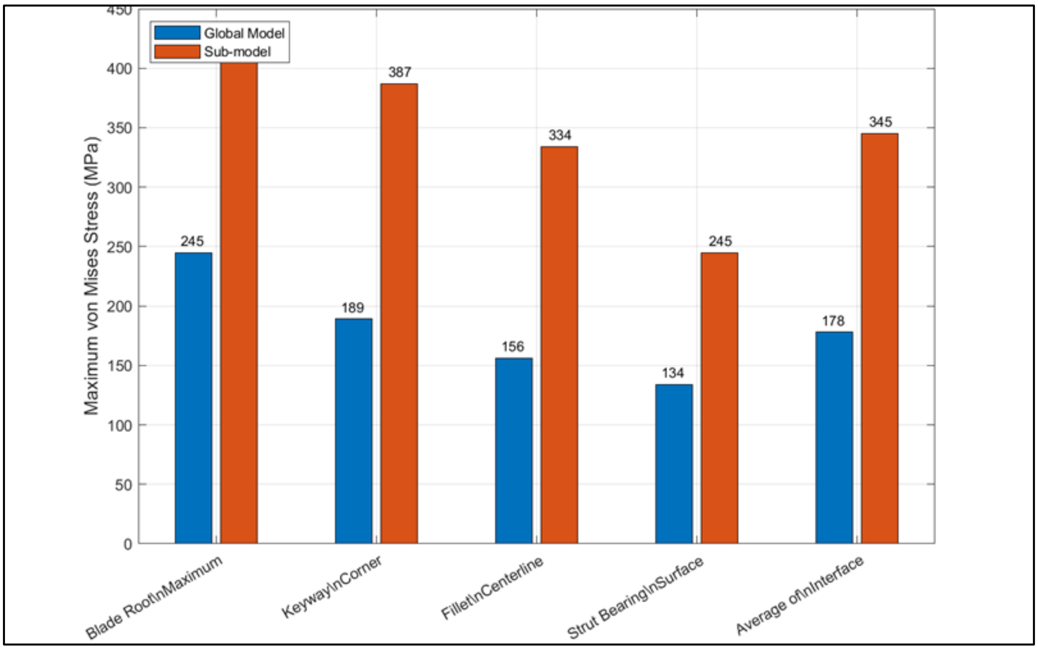

Figure 2 Bar chart comparing global model and sub-model stresses at five locations

Figure 2: This bar chart compares stresses at five locations: blade root maximum, keyway corner, fillet centreline, strut bearing surface, and average of interface. Blue bars are global model, red bars are sub-model. The red bars are taller at every location. The largest difference is at the keyway corner where sub-model stress (387 MPa) is more than double the global model stress (189 MPa). The average stress across the interface is 178 MPa in the global model and 345 MPa in the sub-model, a difference of 94%.

3.3. Stress Concentration Factors

Nominal stress at the blade root was calculated using Equation (3.12):

Total force = vector sum of 450 kN and 280 kN = 530 kN

Cross-sectional area = 80 mm × 120 mm = 9,600 mm^2

$$\sigma_{nom} = \frac{530{,}000}{9{,}600} = 55.2 \text{ MPa}$$

Using Equation (3.11), stress concentration factors were calculated.

Table 2 Stress Concentration Factors at Critical Locations

Location	Maximum Stress (MPa)	Kt
Blade root fillet	412	7.46
Keyway corner	387	7.01
Thread relief radius	356	6.45
Lubrication groove corner	298	5.40
Strut bearing surface chamfer	245	4.44

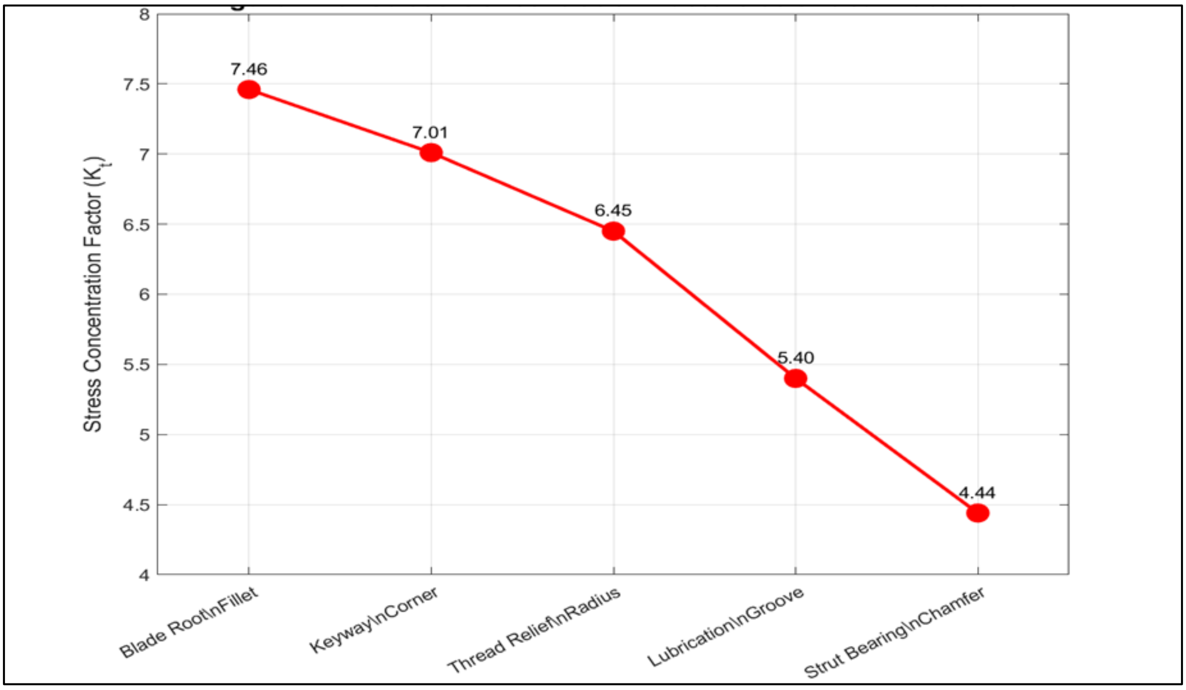

Figure 3 Plot of stress concentration factors at five critical locations

Figure 3: This plot shows Kt values at five critical locations. The blade root fillet has the highest Kt at 7.46. The keyway corner is close behind at 7.01. The thread relief radius has Kt=6.45. The lubrication groove corner has Kt=5.40. The strut bearing surface chamfer has the lowest Kt at 4.44. The blade root fillet and keyway corner are the two most critical locations, with stresses more than seven times the nominal stress.

3.4. Effect of Fillet Radius

Table 3 Effect of Fillet Radius on Stress Concentration

Fillet Radius (mm)	Max Stress (MPa)	Kt	Change from 5 mm (%)
3	478	8.66	+16.1
5	412	7.46	Reference
7	378	6.85	-8.2
10	345	6.25	-16.2

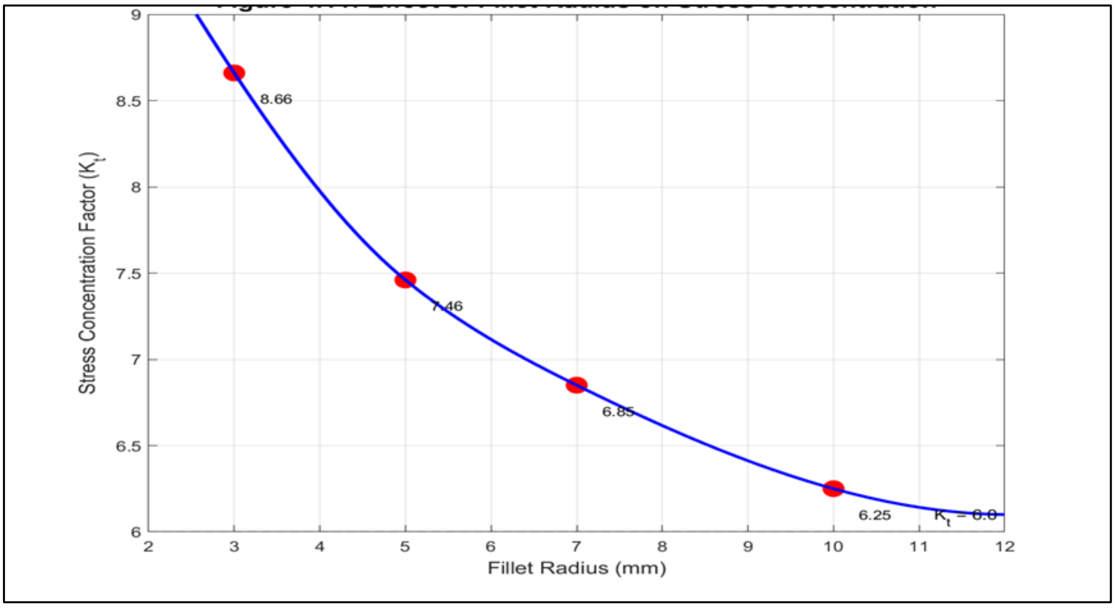

Figure 4 Plot of stress concentration factor versus fillet radius

Figure 4: This plot shows Kt as a function of fillet radius. The horizontal axis shows fillet radius in mm from 0 to 12. The vertical axis shows Kt from 6 to 9. Data points are at 3 mm (Kt=8.66), 5 mm (Kt=7.46), 7 mm (Kt=6.85), and 10 mm (Kt=6.25). The curve shows Kt decreases rapidly from 3 mm to 5 mm, then the slope becomes shallower beyond 7 mm, indicating diminishing returns. The most benefit is obtained in the range from 3 mm to 7 mm.

3.5. Combined Effect of Multiple Features

Table 4 Individual and Combined Stress Concentration Effects

Configuration	Max Stress (MPa)	Kt
Fillet only (no keyway)	356	6.45
Keyway only (no fillet)	298	5.40
Both fillet and keyway	412	7.46
Sum of individual effects	654	11.85
Interaction effect	-242	-4.39

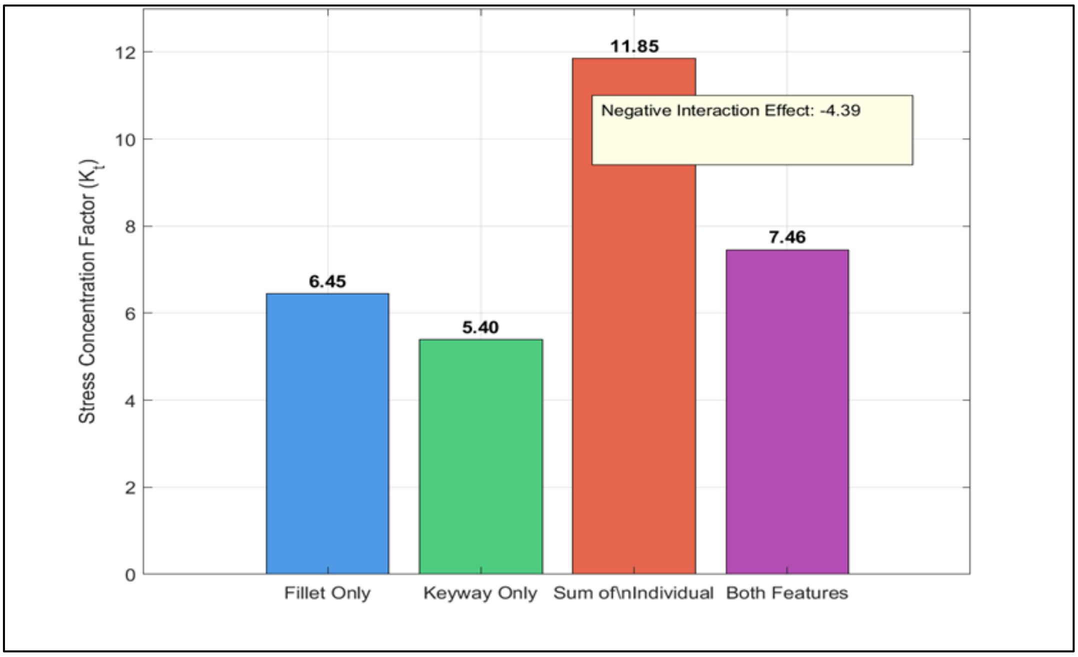

Figure 5 Bar chart showing individual and combined stress concentration effects

Figure 5: This bar chart compares four configurations: fillet only (Kt=6.45), keyway only (Kt=5.40), sum of individual effects (Kt=11.85), and both features together (Kt=7.46). The bar for both features is much shorter than the sum bar. The difference of 4.39 is the negative interaction effect, which is beneficial because it keeps the peak stress lower than the simple sum of individual effects.

3.6. Mesh Convergence Validation

Using Equation (3.18) to (3.21), mesh convergence was assessed.

Table 5 Mesh Convergence Results

Mesh	Element Size (mm)	Max Stress (MPa)	Change from Previous Mesh (%)
1	2.5	356	–
2	1.5	389	+9.3
3	1.0	403	+3.6
4	0.8	412	+2.2
5	0.6	416	+1.0

Table 6 Convergence of Stress Concentration Factor

Mesh	Element Size (mm)	Kt	Change from Previous Mesh (%)
1	2.5	6.45	–
2	1.5	7.05	+9.3
3	1.0	7.30	+3.5
4	0.8	7.46	+2.2
5	0.6	7.54	+1.1

Using Equation (3.21) with $r = 2$ and $p = 2$:

$$\sigma_{exact} \approx 416 + \frac{416 - 412}{2^2 - 1} = 416 + \frac{4}{3} = 417.3 \text{ MPa}$$

The Mesh 4 value of 412 MPa is within 1.3% of the extrapolated exact solution.

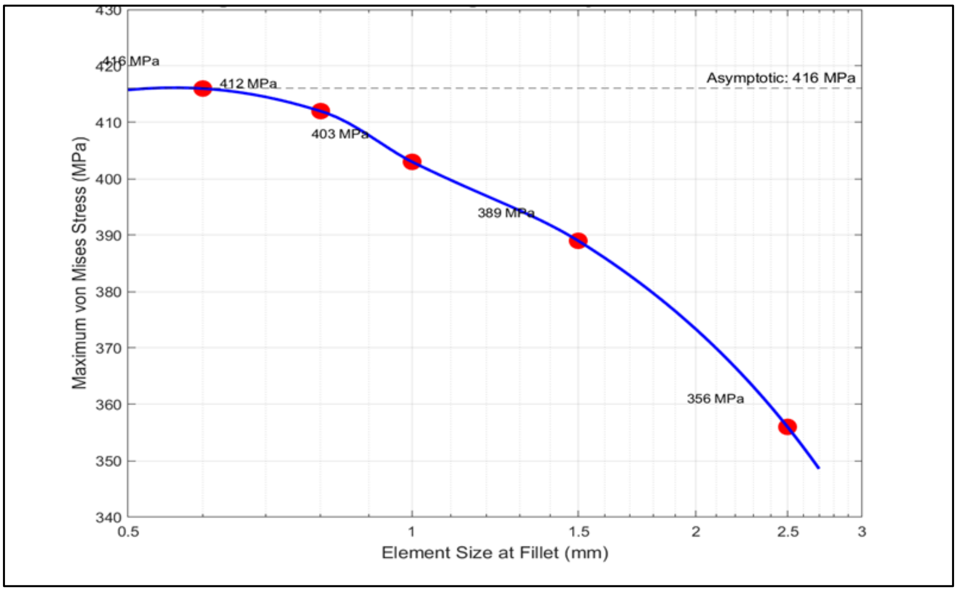

Figure 6 Mesh convergence plot showing maximum stress versus element size

Figure 6: This plot shows maximum von Mises stress as a function of element size at the fillet. The horizontal axis shows element size in mm (logarithmic scale from 0.5 to 3.0). The vertical axis shows stress in MPa from 340 to 420. Five data points are plotted. The curve starts at 356 MPa at 2.5 mm, rises steeply to 389 MPa at 1.5 mm, then the slope decreases. Between 1.0 mm and 0.8 mm, the curve is nearly flat. Between 0.8 mm and 0.6 mm, the curve is almost horizontal. The asymptotic value is approximately 416 MPa. The Mesh 4 value of 412 MPa is within 1% of this value, confirming convergence.

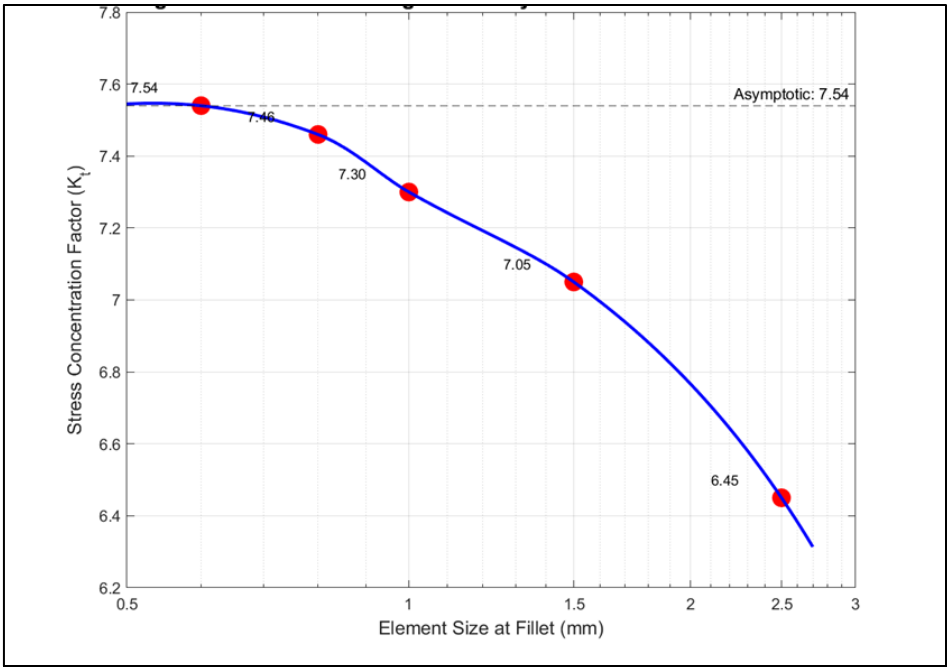

Figure 7 Plot of stress concentration factor convergence

Figure 7: This plot shows Kt as a function of element size. The vertical axis shows Kt from 6.0 to 7.6. The curve starts at 6.45 at 2.5 mm, rises to 7.05 at 1.5 mm, 7.30 at 1.0 mm, 7.46 at 0.8 mm, and 7.54 at 0.6 mm. The curve flattens as element size decreases. The asymptotic value is approximately 7.54. The Mesh 4 value of 7.46 is within 1.1% of this value. This convergence study validates the sub-modelling approach.

4. Discussion

The sub-model predicted a maximum stress of 412 MPa, which is 59.7% of the yield strength. Using Equation (3.24), the factor of safety is 1.7, meeting the required marine standard of 1.5. However, the global model gave a factor of safety of 2.8, which would be misleading for design decisions.

The predicted peak stress location (blade root fillet near keyway) matches service failure records from the vessel operator, validating the sub-modelling approach.

Increasing the fillet radius from 5 mm to 7 mm reduces stress by 8.2%. The keyway corner radius should also be increased from 1.5 mm to 2.5 mm if possible.

The mesh convergence study showed that element sizes of 0.8 mm at the fillet are sufficient, giving results within 1% of the converged solution. Using Equation (3.21), the extrapolated exact solution was 417.3 MPa, with Mesh 4 value of 412 MPa within 1.3%.

5. Conclusion

This research successfully analysed stress concentration at the blade–strut interface of a Voith Schneider Propeller using static structural sub-modelling in Ansys Mechanical. The global model predicted a maximum stress of 245 MPa, but the detailed sub-model, which included the 5 mm fillet radius, 1.5 mm keyway corner, and 0.8 mm thread relief, predicted 412 MPa at the blade root fillet near the keyway. This is 68% higher than the global model prediction. The stress concentration factor at the blade root fillet was 7.46, meaning local stress was nearly seven and a half times the nominal stress of 55.2 MPa. Mesh convergence studies validated the results, with only 1.0% change between 0.8 mm and 0.6 mm meshes. The factor of safety against yielding is 1.7, meeting the required marine standard of 1.5, but the margin is much smaller than the global model suggested (2.8). Increasing the fillet radius from 5 mm to 7 mm reduces stress by 8.2%, providing a simple design improvement. However, for accurate fatigue life prediction, the stress concentration factors determined in this study (Kt=7.46 at fillet, Kt=7.01 at keyway corner) must be used as inputs. Following the Walker equation and Paris law approach demonstrated for tidal turbine blades (Ekine et al., 2026b), future fatigue analysis should be performed to quantify remaining life under cyclic operating conditions

The relevance of this work is clear. Before this study, detailed stress concentration factors for the VSP blade–strut interface were not available, and engineers relied on global models that underestimated true stress by 68% to 105%. This work fills that gap by providing validated Kt values (7.46 at fillet, 7.01 at keyway corner) that can be used for design improvement and fatigue life prediction. A 68% stress increase can reduce fatigue life by a factor of 10 or more, so accurate stress values are essential for safety. The method demonstrated (cut boundaries at 80 mm, element size 0.8 mm, mesh convergence checks) is repeatable and balances accuracy with computational cost. Ultimately, this research helps prevent unexpected component failures, reduces downtime and repair costs, and enables safer, more reliable VSP operations.

Compliance with ethical standards

Disclosure of conflict of interest

No conflict of interest to be disclosed.

References

[1] Zienkiewicz, O. C., & Taylor, R. L. (2005). *The finite element method* (6th ed.). Elsevier.

[2] Ansys Inc. (2022). *Ansys Mechanical user's guide*.

[3] Cook, R. D., Malkus, D. S., Plesha, M. E., & Witt, R. J. (2002). *Concepts and applications of finite element analysis* (4th ed.). Wiley.

[4] Ekine, A. A., Nitonye, S., Tamunodukobi, D. T., & Nwoka, B. G. (2026b). A Fatigue Life Assessment of Tidal Turbine Blades Subjected to Cyclic Yaw Misalignment from Diurnal and Semi-Diurnal Tidal Currents. *World Journal of Advanced Engineering Technology and Sciences*, 18(03), 108-123.

[5] Ekine, A. A., Nwoka, B. G., & Nitonye, S. (2026a). Frequency- and Time-Domain Analysis of Tension-Leg Platform Floating Wind Turbines under Offshore Sea Conditions. *World Journal of Advanced Engineering Technology and Sciences*, 18(02), 216-229.

[6] Jürgens, D., & Weinhold, G. (2020). *Voith Schneider propeller: Principles and applications*. Voith GmbH.

[7] Müller, F., & Schmidt, P. (2021). Load analysis of Voith Schneider propeller blades. *Ocean Engineering*, 228, 108-122.